Real-Time Fluorescence Measurement for Droplet Generation and Signal Detection in a Cylindrical Tube

Shaw-Hwa Parng,* Li-An Wu, Chien-Chih Kuo, Ping-Jung Wu, Yu-Yin Tsai, and Chih-Hung Lee

ACCESS | Metrics & More | Article Recommendations | Supporting Information

ABSTRACT: This study provides an approach for generating droplets in a cylindrical tube. This creative design utilizes a single tube to generate droplets for the emulsion polymerase chain reaction (PCR). We fabricated the multi-layered tube and detected samples in 1 mm microchannel length for the minimum disposable material used for droplet signal analysis. In this research, we verify the validity of the non-planar droplet chip with a single driving pump by experimentally analyzing the light intensity of the liquids during droplet processing in real time. Experimental observation shows that droplet diameter from 150 to 285 μm was obtained by the cylindrical tube with different dispersed liquid and gas pressure settings. Average size of droplets decreased by approximately 37% as the dispersed phase liquids change at the same flow pressure of 50 mbar. In this study, the effects of the laser site, 6-carboxyfluorescein (6-FAM) dye buffer, DNA reagent, and driving pressure are analyzed directly by the signal recorded during droplet generation in the cylindrical tube. Finally, we have developed a real-time detection method to count exon 19 deletion mutations of epidermal growth factor receptor (EGFR) in a droplet using a cylindrical tube. Two digital droplet PCR methods were compared in measuring the copy numbers of EGFR with the same target DNA concentration of 10^5 copies/μL.

Generate and detection droplets in a cylindrical tube
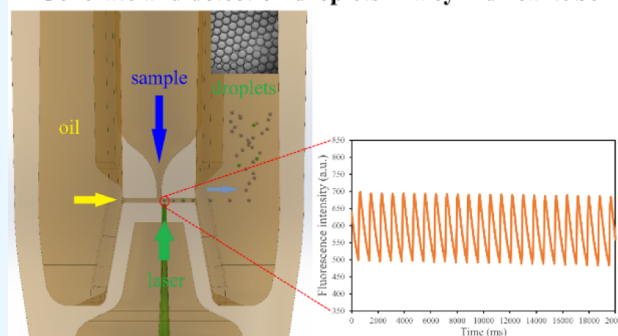
INTRODUCTION

The droplet digital polymerase chain reaction (ddPCR) is a method of performing absolute quantification for nucleic acid molecules.[1] In a general ddPCR, a droplet generator was used to divide a sample into hundreds or even tens of thousands of picoliter level or even femtoliter level[2] single water-in-oil droplets. In these small droplets, some of the droplets do not contain nucleic acid molecules[3] or only contain a single cell.[4] Thereafter, PCR amplification is performed on a specimen in the droplets, and then, a fluorescence signal is applied to perform detection and statistical analysis.[5] Compared with a conventional quantitative PCR, the digital PCR demonstrate a high sensitivity, high accuracy, and multi-target quantitative ability.

The planar droplet microchannel was reported by Thorsen et al.[6,7] In recent years, different droplet structures have been proposed to produce monodisperse droplets.[8−11] Droplet-based PCR assays are particularly well suited for the analysis of clinical samples where the DNA fragments represent only a small fraction of the total DNA. For example, the commercial droplet generator with a PCR system was used in DNA copy number variation.[12−14] A number of disposable chips were used in the ddPCR process, including droplet generation, thermocycling, reinject, and analysis.

For example; a method of using a commercial ddPCR machine for detection may include the following steps:

droplets are generated by using a droplet generator; the generated droplets are placed in a 96-well plate sealer for sealing; the sealed 96-well plate is placed in a PCR machine to perform nucleic acid amplification; and the droplets subjected to the nucleic acid amplification are extracted to a droplet detector to perform optical interpretation. Since each operation process is processed in a different container and a different machine,[14] the sample is liable to have some loss during the transfer process, and process automation is quite difficult.

Meanwhile, the ddPCR process requires a large number of consumables, especially the droplet generator used to generate the droplets, which cannot be reused due to a concern of cross-contamination of specimens, causing the cost of detection to be increased. A two-temperature continuous-flow PCR polymer chip has been constructed by Mohr et al.[15] that takes advantage of the droplet technology to avoid sample contamination and adsorption at the surface.
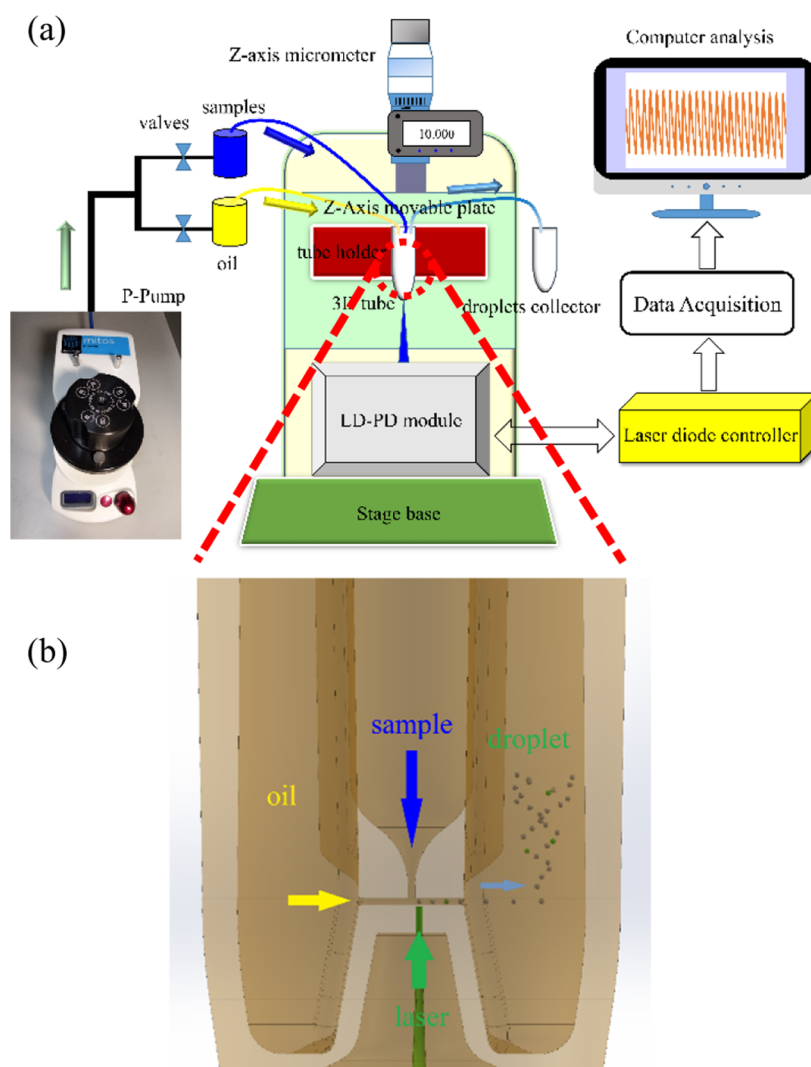
Figure 1. (a) Schematic diagram of the experimental setup using the tubular structure to produce droplets. Sample and oil are driven by the compressed air-driven pump simultaneously. (b) Detail of the local region of the droplet PCR chip where droplets passing through the detection zone under the tube, the droplets signal are detected by the optical detection system.

Beer et al.[16] developed a microfluidic real-time PCR instrument for generating monodisperse microdroplet reactors, including thermal cycling for PCR and detecting real-time amplification in the individual picoliter droplets. Silicon-glass anodic bonded chip with two infusion syringe pumps and off-chip valving system were controlled during the entire PCR reaction. Many recent studies on droplet-based PCR chips are made of polydimethylsiloxane (PDMS) and glass using external syringe pumps. A microscope and a charge-coupled device-camera are usually used for characterization of the droplets. The whole setup is rather bulky, and the collected data are difficult to analyze automatically.

In our previous research,[17,18] we provided a three-dimensional (3D) flow path structure design to form droplets in a multi-layer polypropylene (PP) tube. In this research, we demonstrate the droplets generated in a cylindrical tube and detected by an off-chip laser detection module simultaneously. Not only droplets generation in the PP tube but also the droplets are detected in the same tube. The research first proposes a semiconductor laser diode (LD) module on the same site to detect a droplet in the microchannel of the PP tube.

Most commercial microfluidic droplet generators rely on the planar flow-focusing configuration implemented in polymer or glass chips. In the effort to minimum the chip size, we demonstrate a compact vertical droplet generation and detection system. Furthermore, several potential benefits are realized through multiple sampling and automatic operation.

In this research, the compact integrated system evaluates the real-time measurement of the droplets by various parameters, including the effects of laser site, 6-carboxyfluorescein (6-FAM) dye concentration, and driving pressure. We also investigated the different parameters that have an effect on droplet size distributions. Moreover, we demonstrate the feasibility of applying the 3D cylindrical tube system to detect epidermal growth factor receptor (EGFR) exon 19 deletion mutation.

■ METHODS

Figure 1 illustrates the droplet generation process in the tube. By application of pressure to the inlets, samples and oil are drawn through a vertical channel to a horizontal channel. Then, the droplets were collected in the chamber of the tube. An optical detection system was placed under the micro-

channel, and whether any droplet has passed the microchannel is determined through real-time detection. Therefore, the droplet sizes are controlled by adjusting the pressure driving system in real time.

After the droplets were produced, DNA amplification in the droplets is performed using thermal cycling in the tube. After the PCR test is finished, the pressure driving system will push the droplets to make the droplets to move from the droplet chamber to the oil chamber through the same microchannel. Therefore, the optical detection systems are used again to perform optical signal detection on the droplets passing through the microchannel.

Namely, the steps such as droplet generation of the ddPCR, PCR, droplet detection, and so forth are all performed in the tubular structure without replacing consumables, so that a procedure of the ddPCR may be simplified to reduce the cost.

EXPERIMENTAL SECTION

Flow Setup and Material Preparation. To generate water-in-oil droplets, we utilized a multi-layer microstructure PP tube made by injection molding design, as shown in the previous research.[17,18] There are three holes on the top of the tube, including oil inlet, sample inlet, and droplet outlet. All of the holes are connected with our driving system, as shown in Figure 1a.

As seen in Figure 1a, fluid control was achieved by connecting the chip's three fluid ports to an off-chip valve system. With a good response time and accuracy, the Dolomite Mitos P-Pump was used to create a pulseless liquid flow. The Mitos P-Pump are used directly to provide low air pressure to drive the liquids from the containers. To avoid contamination, the liquid valves on the containers were closed before disconnecting the transfer lines. A pipette is used to transfer 500 μL of chemical liquid and 500 μL of oil in each container. Fluid lines of polytetrafluoroethylene tubes connecting to the multi-layer PP tube were coupled to two-inlet ports driven by a Mitos P-Pump. Droplets leaving the outlet port were collected into a commercial tube.

There are three main chambers and two microchannels in the layout of the tubular structure, as shown in Figure 1b. A 3D flow path structure was fabricated to form droplets with a multi-layer PP tube. The overall dimension of the assembled tube is 18 mm in height and 6 mm in diameter. Each channel was constructed with a built-in 200 μm microchannel in width and a through hole of 100 μm diameter. The multi-layer PP tube design and fabrication have been shown in previous studies.[17,18] The tubes were inserted into the holes of the holder that are made of aluminum alloy.

The oil agent (Bio-Rad Laboratories, Inc.) enters the channel through the inlet for the carrier liquid. The other inlet is for the aqueous liquid. A 10-fold serial dilutions of 6-carboxyfluorescein fluorescent dye (6-FAM, Sigma-Aldrich) were performed in Tris−ethylenediaminetetraacetic acid buffer (10×, pH8.0, Uniregion Bio-Tech, Taiwan). Each sample was measured in duplicate. All samples were kept at room temperature.

RESULTS AND DISCUSSION

Device Setup and Experimental Test. The samples and the oil were loaded into the tube during the experimental research. Then, the droplets were generated with the Mitos P-Pump. An optical detection system was placed under the

microchannel, and whether any droplet passed through the microchannel is determined by a real-time detection system, as shown in Figure 2.
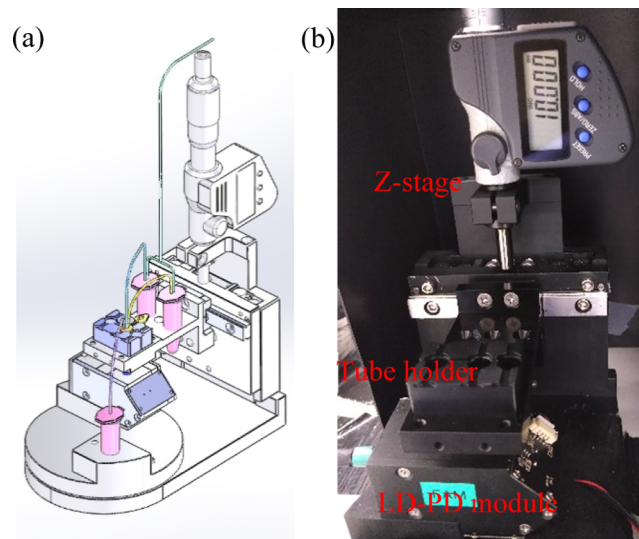
Figure 2. (a) Schematic diagram of the real-time droplet detection system showing the overall layout. (b) Photograph of detection module consists of a tube holder, a fluorescence detector, and a spiral micrometer in a movable Z stage for the droplet measurement in a cylindrical tube.

In order to calibrate our LD and photodiode (PD) detection system (LD−PD module), first, 50 μL of 1 μM 6-FAM was loaded into the microchannel of the cylindrical tube. The fluorescence emission was measured at 520 nm using a 488 nm excitation laser. The fluorescence signals were collected by an optical element and acquired at a speed of 500 points per second for static and kinetics measurement. For detecting the 6-FAM signals, the cylindrical tube holder is positioned and aligned to an optimum detection zone. An increased Z-height is applied when measuring in the middle of microchannel or the other regions of the cylindrical tube. A fixed injection current of 68 mA is supplied by a commercial LD driver (Thorlabs, LDC 202C). Comparing the signal data from various Z heights (Figure S1, Supporting Information), we are able to find the best signal performance and hence achieve an accurate measurement in the cylindrical tube.

In order to quantify the observed signals, we systematically measured the fluorescence signals at various 6-FAM concentrations from 0.1 to 10 μM in the cylindrical tube. A linear curve was fitted to the experimental curve with R^2 = 0.9981, as shown in Figure S2a (Supporting Information). The other linear curves were fitted to the experimental curves with R^2 = 0.9987 and R^2 = 0.9983, as shown in Figure S2b,c, respectively (Supporting Information). Our device provides means to detect 6-FAM fluorescein concentrations down to 0.1 μM. The detection limits are decreased using, for example, a higher power light source excitation.

The high correlation between different 6-FAM concentrations indicates the accurate performance of our detection system. In our device, aqueous droplets are continuously moved by the carrier oil. Oil filled in the channel could be regarded as a background signal during the ddPCR measurement. To investigate all of the possible fluids in droplets, we

Table 1. Results of Recorded Fluorescence Data from Various Samples[a]

samples	oil	6-FAM = 0.1 μM	6-FAM = 1 μM	6-FAM = 10 μM
fitted linear equations	$y = -0.0003x + 153.51$	$y = -0.0556x + 382.19$	$y = -0.3444x + 2264$	$y = -2.364x + 14187$
average (pA)	152.218	368.018	2157.509	13793.93
standard deviation (pA)	1.266	1.652	7.879	70.434
SNR (signal-to-noise ratio)	0	10974.75	68114.98	37789.60
10 log SNR	null	40.339	48.146	45.752

[a]The fitted linear equations represent the fluorescence signals measured for various 6-FAM concentrations at the first recording time. The average and standard deviation represent the three different times of fluorescence signals measured from a variety of 6-FAM concentrations and oil samples in the cylindrical tube.

also compared the performance of our system approach with oil in the same operation procedures.

The measured fluorescence data summary for the four samples is listed in Table 1. In the experiment, the linear fit to the 10 μM of 6-FAM has a faster decaying slope of 2.36, while the linear fit to 0.1 μM of 6-FAM, the slower decaying signal, has a slope of 0.0556 in the same Z height of 10 mm. The higher concentrations of 6-FAM with a faster decaying slope often display a greater standard deviation, for example, 10 μM 6-FAM with a standard deviation of 70.4 pA which is almost nine times greater than that of 1 μM 6-FAM. The 0.1 μM 6-FAM with a smaller standard deviation is almost the same as that of oil background.

The signal-to-noise ratio (SNR) in dB calculated according to standard methods[19]

$$\text{SNR} = \frac{(\overline{S_A} - \overline{S_B})^2}{\sigma_A^2 + \sigma_B^2} \tag{1}$$

and

$$\text{SNR}_{dB} = 10 \ \log \frac{(\overline{S_A} - \overline{S_B})^2}{\sigma_A^2 + \sigma_B^2} \tag{2}$$

where $\overline{S_A}$ and $\overline{S_B}$ are the average fluorescence and background signals, respectively, and σ_A and σ_B are the deviations of each signal.

In this work, we performed analysis of 6-FAM fluorescence intensities in the cylindrical tube to evaluate the signal performance by SNR. The SNR for various 6-FAM concentrations is 40.3, 48.1, and 45.8 dB. The SNR is calculated using eq 2 based on the oil as the background signals. The SNR is inversely proportional to the background signal level. On average, the SNR of 1 μM 6-FAM solution is 16.2% greater than that of 0.1 μM 6-FAM solution. The fluorescence intensity of 1 μM 6-FAM solution is 5.86 times greater than that of 0.1 μM 6-FAM solution. Therefore, the 6-FAM solution at 1 μM is suitable for further droplet fluorescence intensity analysis.

Droplet Size Measurement. All experiments were conducted with the oil agent (Bio-Rad Laboratories, Inc.) as the continuous phase and 10 μM 6-FAM dye buffer or genomic K562 DNA (Promega) PCR sample kit as the dispersed phase. Fluids were actuated into the cylindrical tube using a Mitos P-Pump. A stable gas pressure ranging from 40 to 90 mbar is used to investigate the effect of the droplet size in the cylindrical tube system.

The liquids were driven by the airflow, then, the droplets were collected into a 0.2 mL commercial tube for size measurement. A 20 μL of emulsions was pipetted onto a clean glass slide for observation. The bright-field image is taken with

a digital sCMOS camera (Hamamatsu, C13440-20CU) and a light source (Nikon, LH-M100C-1) on the microscope.

All images were captured using the same exposure time of 2 ms. The 100× total magnification of images is captured by a high-resolution imaging system to recognize spherical droplets from contours. The representative raw images from different parameters are also shown in Figure S3 (Supporting Information). To analyze the droplet size in a captured image, we used ImageJ to detect and measure the droplets in the emulsion.

Table 2 shows the droplet size results with different operation parameters. Droplet sizes are determined in each

Table 2. Summary of Experimental Measurement of Droplet Size Data Sets for 6-FAM Dye Buffer and the DNA Reagent Kit with Various Driving Pressures[a]

exp. mark	liquid	gas pressure (mbar)	mean diameter (μm)	std. dev. (μm)	CV ratio (%)
F-40	6-FAM	40	285.1	27.5	9.7
F-50	6-FAM	50	259.5	21.8	8.4
F-60	6-FAM	60	254.8	7.9	3.1
F-70	6-FAM	70	277.3	10.7	3.9
F-80	6-FAM	80	270.0	15.9	5.9
F-90	6-FAM	90	274.4	28.6	10.4
D-40	DNA reagent	40	227.1	41.4	18.2
D-50	DNA reagent	50	162.1	17.0	10.5
D-60	DNA reagent	60	157.6	10.7	6.8
D-70	DNA reagent	70	160.4	12.9	8.0
D-80	DNA reagent	80	149.7	26.4	17.6

[a]Data sets were selected to show the mean diameter, standard deviation (Std. dev.), and coefficient of variation (CV ratio) of droplet size distributions.

laboratory by following a standard testing method. It can be seen that the average diameter of 6-FAM droplets was 255–285 μm. The presented average diameter of DNA droplets ranged from 150 to 227 μm.

van Dijke et al.[20] report the effect of viscosity of both continuous and to-be-dispersed phases on the microchannel. At low viscosity ratios, the droplets become larger. Since the DNA reagent kit has a higher viscosity than the 6-FAM buffer (the viscosity of the buffer is approximately 1 cP), then the final droplet diameter would be smaller for the same gas pressure driving in the cylindrical tube. Meanwhile, the change in gas pressure did not significantly alter the droplet size in oil.
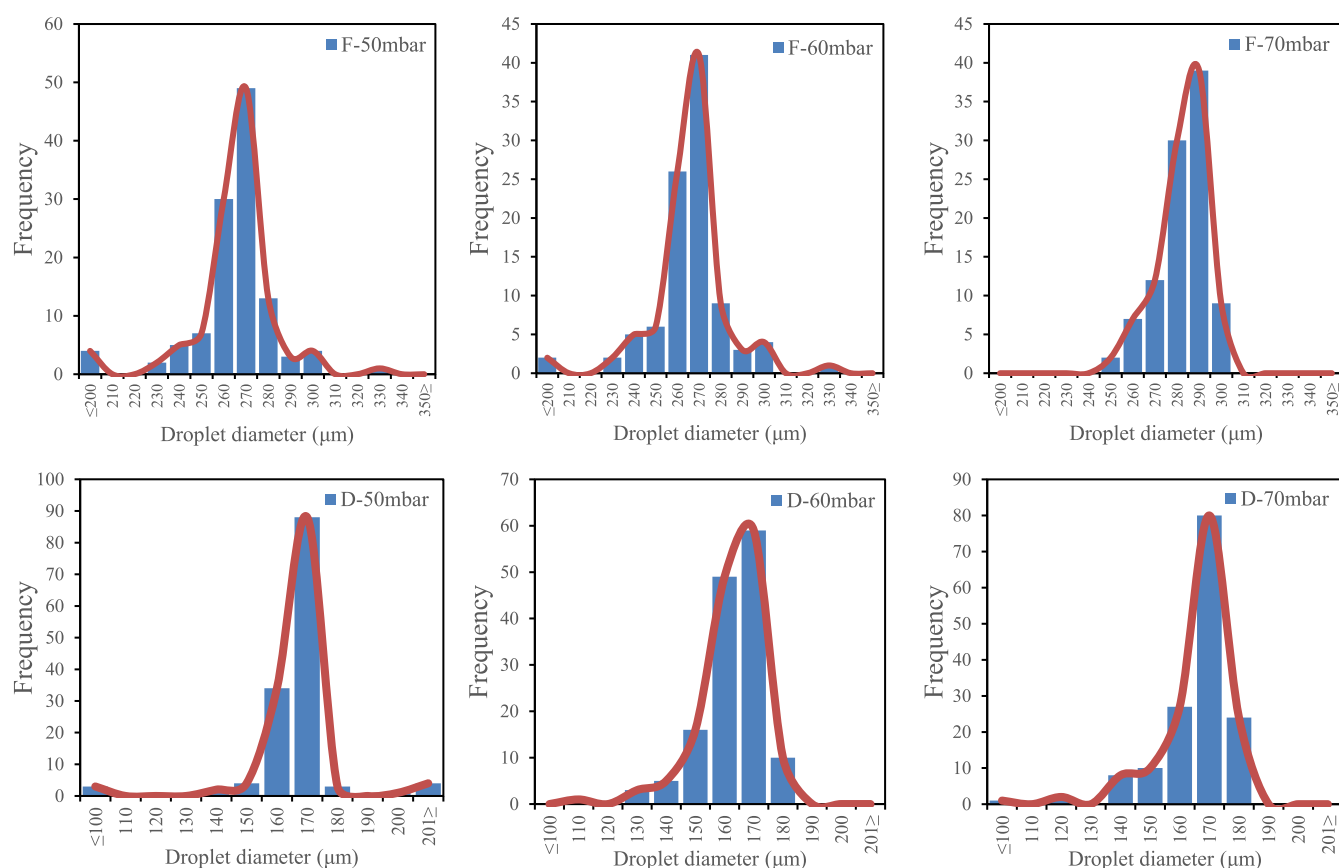
Figure 3. Experimental droplet generation data sets showing histograms for 6-FAM dye buffer (top row) and DNA reagent kit (bottom row) and a smooth curve for the droplet size distributions with various gas pressures.

A uniform distribution of droplet size was obtained at gas pressure of 50−70 mbar, as listed in Table 2. At stable gas pressure ranges, the droplet size standard deviation would be less than 20 μm, and the coefficient of variation would be less than 10%. As we can see in Table 2, the standard deviation of droplet diameter at the higher or the lower gas pressure shows larger variability between laboratories. The higher or lower gas pressure causes the worse droplet size distribution (CV > 10%) under instability conditions. The DNA reagent droplet results showed that within a set pressure range, with an increase in the gas pressure, the droplet size decreased. However, the 6-FAM droplets did not fit this trend under the same range of gas pressures.

Figure 3 shows the histograms of droplet size distribution count with a smooth curve. Histograms show about 100 droplet size distributions produced by the stable gas pressure range for each laboratory. The histogram divides the droplets size counts into 12 or 16 equal segments in droplet diameter measured ranges along the horizontal axis. The heights of the vertical bars correspond to the droplet counts in each range. The symmetric and unimodal histogram means the uniform emulsions are produced at stable gas pressure ranges. Based on the 6-FAM droplets results, the 95% confidence interval for mean droplet diameter ranged from 256 to 263 μm at the stable gas pressure of 50 mbar. For the DNA reagent droplets at the same gas pressure range, the mean droplet diameter for a 95% confidence interval is in between 159 and 165 μm. The average droplet diameter reduced from 259.5 to 162.1 μm (37.5% decrease) as the dispersed liquids change at the same gas pressure of 50 mbar. This result indicates that the viscosity

of the dispersed liquid is one of the dominate factors in the droplet generation.

Droplets Flow Signal Measurements. To further demonstrate the detection system, we have used the cylindrical tube with a Mitos P-Pump using oil and 6-FAM solution to create droplet flow. We have constructed a PD sensor together with an 8 bit analog-to-digital converter for fluorescence signal measurement in the cylindrical tube. For the experimental tests, software AccessPort was used to transfer real-time data via the serial ports. The default 115,200 baud rate setting is designed for a shorter cable length to the data transmission. The signals were obtained at a fixed rate of 500 Hz.

Comparing the high throughput of droplets in the planer microchannel,[21] we characterize the droplet signal analysis at a low throughput in a cylindrical tube. Dangla et al.[22] developed a confinement gradient to produce the droplets providing far more reproducible and robust droplet sizes. This was found to be particularly true when the fluids were driven by a constant pressure source, rather than by syringe pumps.

T-junction and flow-focusing droplet generation are the most widely used techniques in planar microchannels. For example, the channel length for the continuous phase is 15 mm and for the dispersed phase is 5 mm.[23] Our research offers an alternative approach to minimize the droplet microfluidic chip. Droplets to be generated and signals are detected in a disposable injection tube. Real-time counts from individual droplets are a challenge in a compact microchannel size of 0.2 mm width, 0.1 mm depth, and 1 mm length. Another challenge is signals recorded in the dynamic flowing of droplets.

In order to observe the effects of fluorescence variation during the droplet flow procedure, we have special interest in the lower operating pressures in the range of 25−50 mbar. After changing each of gas pressure of the flow parameter, we waited for an appropriate amount of time of about 30 s before taking signal measurements in order to get a steady-state flow. The minimum pressure to produce droplets is 20 mbar of water in the PDMS−glass chip.[23]

The Laplace pressure ΔP is used to determine the pressure difference in spherical shapes of droplets.

$$\Delta P_{\text{Laplace}} = \sigma\left(\frac{2}{R}\right) \tag{3}$$

where $\sigma \approx 30$ mN/m is the oil−water interfacial tension and $R = 50$ μm is the diameter of the channel. This yields $\Delta P_{\text{Laplace}} = 12$ mbar and is close to the minimum pressure setting in our research. In our experiments, unstable droplets occur at an air pressure of less than 20 mbar. Therefore, four pressures (25, 30, 40, and 50 mbar) were applied to the both inlets of the cylindrical tube. The flowing droplet signal detected by our LD−PD detection module for each driving air pressure is shown in Figure S4 (Supporting Information).

As we can see in Figure 4a, the peak-to-peak amplitude of fluorescence intensity increases with the increase of the higher driving pressure from 25 to 50 mbar.

Comparison of the 6-FAM signal with a moving droplet form, a fully filled 6-FAM solution without flow in the microchannel would produce a higher fluorescence intensity (Tables 1 and 3). The linear curve fitted equations of the static

and moving signals are expressed as $y = -0.3444x + 2264$ and $y = -0.0006x + 592.72$, respectively. On average, only 26.2% of 6-FAM fluorescence intensity is acquired as the droplets flow in the microchannel of the tubular chip. The slower linear regression is related to the smaller signal decay of 6-FAM solution with a moving droplet form. Moreover, the larger the driving pressure, the greater the variation of the measured signal toward big changes during the droplet moving.

An experimental comparison with different driving pressures is shown in details in Figure 4b. When a droplet is moving along the microchannel, the sum of a droplet cycle time (t) is equal to the approaching time (t_1) and the departing time (t_2).

$$t = t_1 + t_2 \tag{4}$$

As droplets pass through the detection zone, the 6-FAM fluorescence signal is received by the LD−PD detection module. The fluorescence intensity of droplet increases quickly as the droplet enters the detection zone. Furthermore, the fluorescence intensity of droplet decreases slowly when the droplet passes through the detection zone. It is noted that the droplet approaching time and departing time were not equal. A significant change in the fluorescence signal was observed after various driving pressures are applied to the system. For the lower driving pressures of 25−30 mbar, the droplet approaching time is about 15% of the total droplet cycle time. However, the droplet approaching time is about 80% of the total droplet cycle time at the higher driving pressures of 40−50 mbar. The experimental results indicate that the higher the driving pressure, the faster the droplet travels in the microchannel. Therefore, the droplet departing time decreases during droplet movement due to the increased higher driving pressure.

Kanik et al.[24] demonstrated that the droplet size has a significant effect on the output signal with a fiber-based microfluidic system. Increasing the droplet size increases the output signal. From fluorescence signal observation with different driving pressures, the peak-to-peak intensity enlarged as the driving pressure increased.

As shown in Figure 4b, the approaching time (t_1) is 0.131 s, and the departing time (t_2) is 0.691 s at a gas pressure of 30 mbar. However, the approaching time (t_1) is 0.414 s, and the departing time (t_2) is 0.109 s at gas pressure of 50 mbar. The higher the approaching time, the greater will be the peak-to-peak fluorescence intensity, as shown in Table 3. In contrast, the less approaching time means a weaker fluorescence intensity acquired during the recording time. As shown in Figure 4a, the peak-to-peak fluorescence intensities drop over time for 25 and 30 mbar. The higher gas pressure provides the higher flow rate of 6-FAM droplets. As shown in Figure S4, the peak-to-peak fluorescence decay is determined directly from the slope of the fitted lines. The fluorescence decay slope of the higher gas pressures becomes 10 times faster than that of the lower gas pressures. This means that stronger fluorescent droplets are also produced in higher gas pressures.

Figure 5 shows the relation between the measured droplet cycle time and the driving pressure. The dashed line is linear fitting function. Higher droplet driving pressure leads to a higher flow rate, and consequently a larger number of droplets would be generated in the same period of time.

The liquid flow rate was estimated based on the Hagen−Poiseuille equation
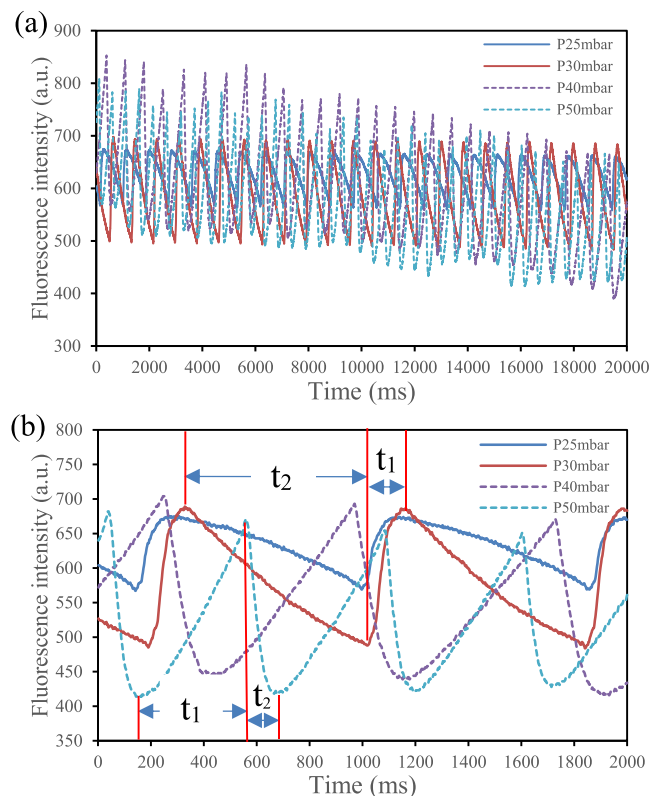
Figure 4. (a) Results of fluorescence signal measurement for droplets generated by air pressure ranges from 25 to 50 mbar. (b) Detailed fluorescence signal measurement for droplets generated by air pressure ranges from 25 to 50 mbar.

Table 3. Droplets of 1 μM 6-FAM Solution Generated by Various Gas Pressures and Each Fluorescence Data Recorded for a Duration of 20 s[a]

pressure	25 mbar	30 mbar	40 mbar	50 mbar
fitted linear equations	$y = -0.0006x + 633.53$	$y = -0.0006x + 592.72$	$y = -0.0087x + 689.35$	$y = -0.0069x + 638.22$
quantity (N)	23	24	28	40
average (pA)	105.217	199.083	272.077	244.1
standard deviation (pA)	1.565	1.976	18.229	20.736

[a]The average and standard deviation represent the peak-to-peak amplitude of fluorescence intensity measured in the cylindrical tube.
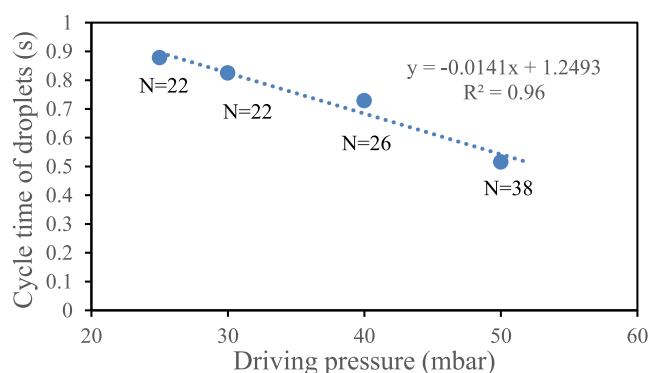
Figure 5. Droplet cycle time as a function of the driving pressure of the inlets. N represents the number of droplet signals that were measured in the cylindrical tube for 20 s.

$$Q = \frac{\pi R^4 (p_1 - p_2)}{8 \mu L} \tag{5}$$

In the Hagen–Poiseuille equation, Q is the volumetric flow rate, $(p_1 - p_2) = \Delta p$ is the pressure difference between the two ends, μ is the dynamic viscosity of the fluid, and R and L are the radius and length of the microchannel. Considering the same flowing model in the chip, the flow rate is proportional to the pressure difference.

Droplet PCR Measurement Results. To validate the sensitivity of our LD-PD module, the DNA amplification in droplets was analyzed in the cylindrical tube. A QX200 Droplet Digital PCR System (Bio-Rad) was used for droplet generation and PCR process. The droplet sample was generated in a 20 μL of reaction volume containing 2 μL of EGFR exon 19 deletion mutations, 10^5 copies/μL of 2 μL of genomic K562

DNA, 6.59 μL of DNase/RNase-free distilled water, and 10 μL of 1× PCR master mix (Thermo).

Genomic K562 DNA (Promega) samples are purified from a subculture of the human chronic myelogenous leukemia cell line. For each test, EGFR exon 19 deletion is considered as mutational hot spots and was individually amplified by PCR using a pair of corresponding primers and probes. Each droplet reaction contained duplex TaqMan assay reagents of the wild-type and mutant genes.

The PCR conditions were as follows: initial denaturation at 95 °C for 10 min, 41 cycles at 94 °C for 30 s, 50 °C for 1 min, and 72 °C for 20 s.

The PCR droplets were injected into the cylindrical tube using the Mitos P-Pump for signal measurement. The driving pressure was set in a range of 50−80 mbar for the liquid phase. Each PCR droplet was measured using the LD−PD module. Figure 6 shows the histograms of the detection peak-to-peak amplitude for negative and positive droplets with different driving gas pressures. The curves show smooth fits to the respective histograms. The peak-to peak value is the difference between the maximum positive and the maximum negative amplitudes of the measured current waveform, as shown in Figure S5 (Supporting Information).

For the current measurement of negative PCR droplets, most of the measured current points are concentrated between 235 and 255 pA. It can find and count over 200 obvious peaks with 30,000 data points for the recording time of 60 s. The histogram divides the peak-to-peak current amplitude, ranging from 0 to 40 pA into 10 equal segments for the horizontal axis. The heights of the vertical bars correspond to the peak-to-peak current counts in each range.

Figure 6a shows the histogram of peak-to-peak current for nontemplate control (NTC) in droplets. It has one peak between 11 and 18 pA. The single peaked curve of the peak-to-
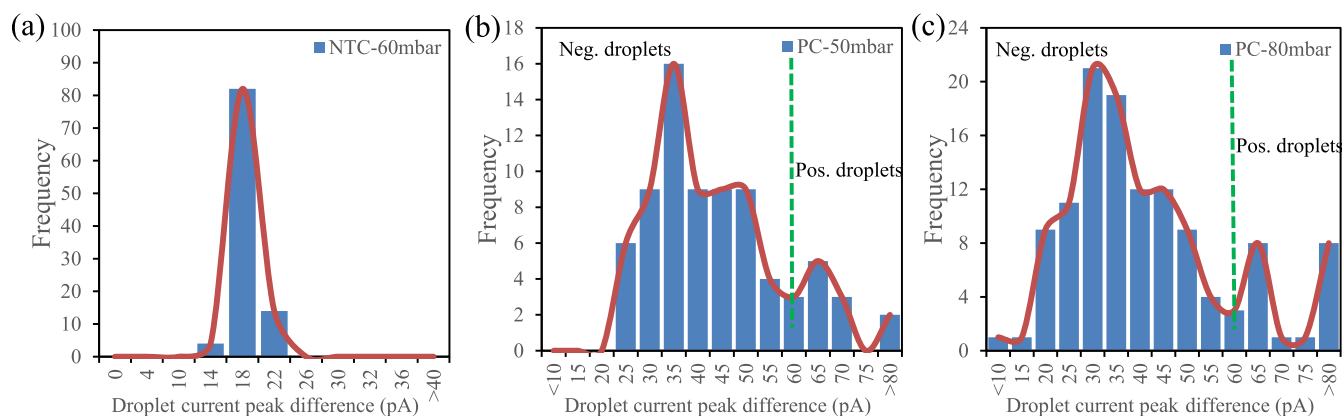
Figure 6. (a) Histogram of peak-to-peak current for the nontemplate PCR droplets (without DNA template) measured in a cylindrical tube. (b) Histogram of peak-to-peak current for positive PCR droplet (with EGFR exon 19 deletion) flow at a pressure of 50 mbar measured in a cylindrical tube. (c) Histogram of peak-to-peak current for positive PCR droplet flow at a pressure of 80 mbar measured in a cylindrical tube.
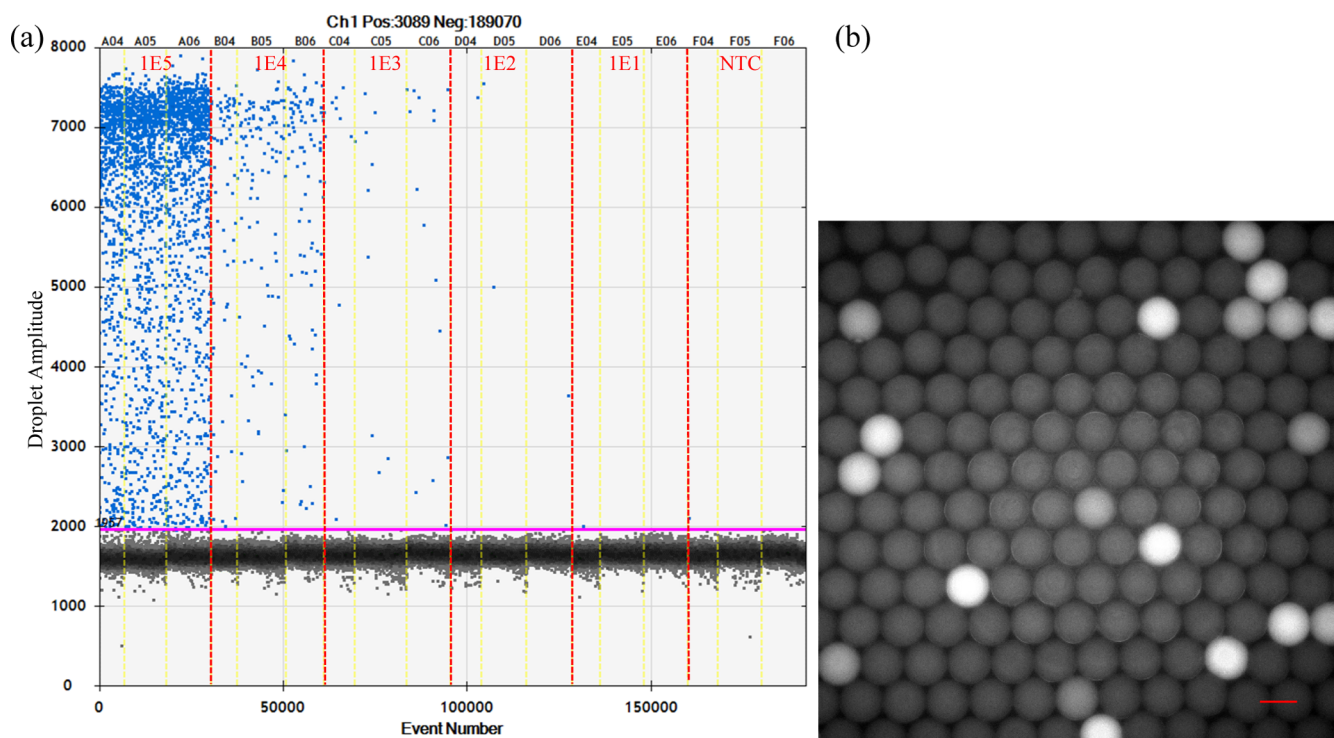
Figure 7. (a) Series of 10-fold dilutions for positive PCR droplets were analyzed using a QX200 ddPCR system (Bio-Rad). The pink horizontal line represents the intensity threshold used to classify negative droplets. The yellow vertical lines show the well boundaries with target DNA concentrations (red vertical lines), ranging from 0 to 10^5 copies/μL. (b) Fluorescence image of positive PCR droplets that self-assembled into a hexagonally patterned cluster in a PDMS−glass chip. The scale bar is 100 μm.

peak amplitude is close to symmetric in the histogram. There are no extreme values outside that range. The mean value of peak-to-peak amplitude is 14.8 pA.

Comparison of the background noise effect, the continuous phase flow with oil at the gas pressure of 50 mbar, and the resulting currents are recorded in Figure S5a,b (Supporting Information). The average background peak-to-peak amplitude is about 5.5 pA. The average NTC droplets peak-to-peak current is 2.7 times larger than that of the background noise. The response current increased with the total projected area of droplets passing through a detection zone. Therefore, the negative droplets were identified as positive pulses in the measured currents.

The current signals for droplets with 10^5 copies/μL of DNA concentration were also in-flow measured in a cylindrical tube (Figure S5c,d, Supporting Information). Figure 6b shows the histogram of peak-to-peak current for positive PCR droplets at a flow pressure of 50 mbar. On average, peak pulse frequency is around 1.25 Hz. As can be seen in Figure 6b, the histogram divides the peak-to-peak current amplitude ranging from 10 to 80 pA into 15 equal segments for the horizontal axis. The heights of the vertical bars correspond to the peak-to-peak current counts in each range.

Two clearly separate groups are visible in the bimodal histogram shown on the same graph. One group represents the lower measured currents of negative droplets, and the other group represents the higher measured currents of positive droplets. The dash-dotted green line represents the peak-to-peak current threshold (about 60 pA) used to classify negative droplets. Negative droplets (without DNA template) are seen on the left side of the graph. The peak-to-peak current of each

negative droplet is ranging from 3 to 60 pA. The mean peak-to-peak current of negative droplets is 37.9 pA.

The positive droplets (containing mutant, wild-type, or both alleles) are seen on the right side of the same graph. For droplets that contain mutant genes, specific cleavage of TaqMan probes generates a strong fluorescence signal. Each droplet has an intrinsic fluorescence signal, resulting from the imperfect quenching of the fluorogenic probes enabling detection of positive droplets. There are 10 peak-to-peak measured currents, which are above the threshold of 60 pA and were to be considered as positive droplets. The mean peak-to-peak current of positive droplets is 68.8 pA. The mean peak-to-peak measured currents of positive droplets increase about twice that of negative droplets. The ratio of positive droplets to the total number of droplets is 13.3%.

Figure 6c shows the multi-peak histogram of peak-to-peak current for positive PCR droplets at a flow pressure of 80 mbar. On average, the peak pulse frequency is around 2 Hz. There are 18 peak-to-peak measured currents, which are above the threshold of 60 pA and were to be considered as positive droplets. The ratio of positive droplets to the total number of droplets is 15%.

Figure 7 shows a 10-fold serial dilution of the target DNA concentration, ranging from 0 to 10^5 copies/μL. Both positive and negative PCR droplets were analyzed using a QX200 ddPCR system (Bio-Rad). For each target DNA concentration, three replicate measurements were performed using three duplicate droplet wells.

Every data point corresponds to a droplet. Each droplet with mutant of EGFR exon 19 deletion DNA is shown as a producer in the blue labeled point. Each droplet with wild-type of EGFR exon 19 deletion DNA is shown as a producer in the

green labeled point. For the target DNA concentration of 10^5 copies/μL, there are 2783 positive droplets in three sample wells counted in total of 30,660 droplets. Therefore, the ratio of positive to total droplets is 9.08%. The positive and negative ddPCR results for the mutant and wild-type of EGFR exon 19 deletion DNA are also shown in Figure S6 (Supporting Information).

Due to the digital PCR droplet observation in a transparent chip, a PDMS cover which has a microchannel of 2 mm in width and 110 μm in depth was bonded onto the PDMS substrate following O_2 plasma treatment. The PDMS cover was fabricated in two stages, the first master pattern coated on a silicon substrate using soft lithography and the second, PDMS was cast and cured on the master pattern by replica molding. The PCR amplified droplets were manually transferred to a PDMS–PDMS chip with a pipette for fluorescence observation.

Figure 7 shows the PCR-amplified droplets, the target DNA concentration of 10^5 copies/μL, with green fluorescence image taken at 10× magnification in the PDMS–PDMS chip. Due to the confinement in channel depth, the droplets spread out in a single layer in the PDMS–PDMS chip. After the droplets settled down in the imaging well and formed a monolayer, images were taken in less than 1 min in order to reduce the fluorescence decay and to keep the droplets in spherical shape.

For all images processing, we used ImageJ to count the number of positive droplets and negative droplets in the chamber. From the fluorescence image of the same PCR droplets in Figure 7b, the positive rate of droplets is 10.2% (17/167). The positive rate counted in an image is closer to the value of 9.08% measured using the Bio-Rad QX200 droplet reader. In addition, there are some positive droplets that do not emit enough fluorescence intensity and are also observed in Figure 7a,b.

We have examined the signal of the positive and negative droplets for the same target DNA concentration of 10^5 copies/μL. As shown in Figure 6, we calculate the positive droplet ratios in the range from 13.3 to 15% at different flow pressures of 50 and 80 mbar in a cylindrical tube. The ratio of positive to total droplets is closer to the results of the Bio-Rad QX200 digital PCR platform. We demonstrate that the digital droplet PCR results from our LD–PD system are used to directly measure the rare mutant target DNA in a cylindrical tube.

CONCLUSIONS

We provide a 3D tubular structure with a multi-layer injection parts to form droplets that are detected in the same tube in real time. We have established a compact droplet detection module for the 6-FAM and EGFR exon 19 deletion in the cylindrical tube. The average droplet diameter reduced from 259.5 to 162.1 μm as the dispersed liquids change at the same gas pressure of 50 mbar.

The experimental observation of the droplet generation process indicated that the droplet generation frequency depends on the driving pressure in the cylindrical tube. The in-flow signals measured in the cylindrical tube were compared with that of a QX200 platform for droplets of 10^5 copies/μL DNA concentration. The positive droplet ratios of the same concentration of EGFR exon 19 deletion measured in our system and QX200 platform are 13.3 and 9.08%, respectively.

In this research, droplet generation and real-time detection were performed in the single tubular structure without replacing with a different consumable container or a reaction slot. We have developed a simple droplet cylindrical tube for the simultaneous detection of rare mutation DNA within droplets.

ASSOCIATED CONTENT

Supporting Information

The Supporting Information is available free of charge at https://pubs.acs.org/doi/10.1021/acsomega.2c07246.

The fluorescence signal of performance evaluation in the cylindrical tube for static and in-flow was measured in supplementary material. Droplets raw images from different parameters are shown in supplemental figures. The signals for 6-FAM and DNA droplets were experimental analyzed and compared with commercial droplet reader. (PDF)

AUTHOR INFORMATION

Corresponding Author

Shaw-Hwa Parng − *Biomedical Technology and Device Research Laboratories, Industrial Technology Research Institute, Hsinchu 310401, Taiwan;* ● orcid.org/0000-0002-8853-1660; Email: antonio@itri.org.tw

Authors

Li-An Wu − *Biomedical Technology and Device Research Laboratories, Industrial Technology Research Institute, Hsinchu 310401, Taiwan*

Chien-Chih Kuo − *Biomedical Technology and Device Research Laboratories, Industrial Technology Research Institute, Hsinchu 310401, Taiwan*

Ping-Jung Wu − *Biomedical Technology and Device Research Laboratories, Industrial Technology Research Institute, Hsinchu 310401, Taiwan*

Yu-Yin Tsai − *Biomedical Technology and Device Research Laboratories, Industrial Technology Research Institute, Hsinchu 310401, Taiwan*

Chih-Hung Lee − *Biomedical Technology and Device Research Laboratories, Industrial Technology Research Institute, Hsinchu 310401, Taiwan*

Complete contact information is available at:
https://pubs.acs.org/10.1021/acsomega.2c07246

Author Contributions

S.-H.P. and L.-A.W. conceived the concept and performed experiments. C.-K. and P.-J.W. carried out the optical device and measurement system. Y.-Y.T. and C.-H.L. contributed to the reagent preparation and PCR droplet analysis. All authors reviewed and commented on the manuscript.

Notes

The authors declare no competing financial interest.

REFERENCES

(1) Vogelstein, B.; Kinzler, K. W. Digital PCR. *Proc. Natl. Acad. Sci. U.S.A.* **1999**, *96*, 9236−9241.

(2) Leman, M.; Abouakil, F.; Griffiths, A. D.; Tabeling, P. Droplet-based microfluidics at the femtolitre scale. *Lab Chip* **2015**, *15*, 753−765.

(3) Ahmed, R.; Jones, T. B. Dispensing picoliter droplets on substrates using dielectrophoresis. *J. Electrost.* **2006**, *64*, 543−549.

(4) Luo, C.; Yang, X.; Fu, Q.; Sun, M.; Ouyang, Q.; Chen, Y.; Ji, H. Picoliter-volume aqueous droplets in oil: electrochemical detection and yeast cell electroporation. *Electrophoresis* **2006**, *27*, 1977−1983.

(5) Kiss, M. M.; Ortoleva-Donnelly, L. O.; Beer, N. R.; Warner, J.; Bailey, C. G.; Colston, B. W.; Rothberg, J. M.; Link, D. R.; Leamon, J. H. High-throughput quantitative PCR in picoliter droplets. *Anal. Chem.* **2008**, *80*, 8975−8981.

(6) Thorsen, T.; Roberts, R. W.; Arnold, F. H.; Quake, S. R. Dynamic pattern formation in a vesicle-generating microfluidic device. *Phys. Rev. Lett.* **2001**, *86*, 4163.

(7) Quake, S. R.; Scherer, A. From micro- to nanofabrication with soft materials. *Science* **2000**, *290*, 1536−1540.

(8) Roumpea, E.; Kovalchuk, N. M.; Chinaud, M.; Nowak, E.; Simmons, M. J. H.; Angeli, P. Experimental studies on droplet formation in a flow-focusing microchannel in the presence of surfactants. *Chem. Eng. Sci.* **2019**, *195*, 507−518.

(9) Saqib, M.; Şahinoğlu, O. B.; Erdem, E. Y. Alternating droplet formation by using tapered channel geometry. *Sci. Rep.* **2018**, *8*, 1606.

(10) Zhu, P.; Wang, L. Passive and active droplet generation with microfluidics: a review. *Lab Chip* **2017**, *17*, 34−75.

(11) Zhang, J. M.; Ji, Q.; Duan, H. Three-dimensional printed devices in droplet microfluidics. *Micromachines* **2019**, *10*, 754.

(12) Chen, F.; Zhan, Y.; Geng, T.; Lian, H.; Xu, P.; Lu, C. Chemical transfection of cells in picoliter aqueous droplets in fluorocarbon oil. *Anal. Chem.* **2011**, *83*, 8816−8820.

(13) Miotke, L.; Lau, B. T.; Rumma, R. T.; Ji, H. P. High sensitivity detection and quantitation of DNA copy number and single nucleotide variants with single color droplet digital PCR. *Anal. Chem.* **2014**, *86*, 2618−2624.

(14) Pinheiro, L. B.; Coleman, V. A.; Hindson, C. M.; Herrmann, J.; Hindson, B. J.; Bhat, S.; Emslie, K. R. Evaluation of a droplet digital polymerase chain reaction format for DNA copy number quantification. *Anal. Chem.* **2012**, *84*, 1003−1011.

(15) Mohr, S.; Zhang, Y. H.; Macaskill, A.; Day, P. J. R.; Barber, R. W.; Goddard, N. J.; Emerson, D. R.; Fielden, P. R. Numerical and experimental study of a droplet-based PCR chip. *Microfluid. Nanofluid.* **2007**, *3*, 611−621.

(16) Beer, N. R.; Hindson, B. J.; Wheeler, E. K.; Hall, B.; Rose, K. A.; Kennedy, I. M.; Colston, B. W. On-chip, real-time, single-copy polymerase chain reaction in picoliter droplets. *Anal. Chem.* **2007**, *79*, 8471−8475.

(17) Parng, S. H.; Wu, P. J.; Tsai, Y. Y.; Hong, R. S.; Lee, S. J.Droplet generator in a single tube for DNA amplification. *MicroTAS 2020 virtual online conference M2-203*, 2020.

(18) Parng, S. H.; Wu, P. J.; Tsai, Y. Y.; Hong, R. S.; Lee, S. J. A 3D tubular structure with droplet generation and temperature control for DNA amplification. *Microfluid. Nanofluid.* **2021**, *25*, 56.

(19) Roulet, J. C.; Volkel, R.; Herzig, H. P.; Verpoorte, E.; de Rooij, N. F.; Dandliker, R. Fabrication of multilayer systems combining microfluidic and microoptical elements for fluorescence detection. *J. Microelectromech. Syst.* **2001**, *10*, 482−491.

(20) van Dijke, K.; Kobayashi, I.; Schroën, K.; Uemura, K.; Nakajima, M.; Boom, R. Effect of viscosities of dispersed and continuous phases in microchannel oil-in-water emulsification. *Microfluid. Nanofluid.* **2010**, *9*, 77−85.

(21) Nisisako, T.; Torii, T.; Higuchi, T. Droplet formation in a microchannel network. *Lab Chip* **2002**, *2*, 24−26.

(22) Dangla, R.; Kayi, S. C.; Baroud, C. N. Droplet microfluidics driven by gradients of confinement. *Proc. Natl. Acad. Sci.* **2013**, *110*, 853−858.

(23) Frot, C.; Taccoen, N.; Baroud, C. N. Frugal droplet microfluidics using consumer opto-electronics. *PLoS* **2016**, *11*, No. e0161490.

(24) Kanik, M.; Marcali, M.; Yunusa, M.; Elbuken, C.; Bayindir, M. Continuous triboelectric power harvesting and biochemical sensing inside poly(vinylidene fluoride) hollow fibers using microfluidic droplet generation. *Adv. Mater. Technol.* **2016**, *1*, 1600190.